Journal of Cranio-Maxillo-Facial Surgery 47 (2019) 959–967

Contents lists available at ScienceDirect

Journal of Cranio-Maxillo-Facial Surgery

journal homepage: www.jcmfs.com

Three-dimensional orbital wall modeling using paranasal sinus segmentation

Hannah Kim [a, b], Tae-geun Son [a], Jeonghwan Lee [a], Hyeun A. Kim [a], Hyunchul Cho [a], Woo Shik Jeong [c], Jong Woo Choi [c, d, **], Youngjun Kim [a, b, *]

[a] Center for Bionics, Korea Institute of Science and Technology, Seoul, Republic of Korea
[b] Division of Bio-Medical Science & Technology, KIST School, Korea University of Science and Technology, Seoul, Republic of Korea
[c] Department of Plastic and Reconstructive Surgery, University of Ulsan College of Medicine, Asan Medical Center, Seoul, Republic of Korea
[d] Biomedical Engineering Research Center, Asan Medical Center, Seoul, Republic of Korea

ARTICLE INFO

Article history:
Paper received 21 December 2018
Accepted 25 March 2019
Available online 1 April 2019

Keywords:
Orbital reconstruction surgery
Orbital fracture
Maxillofacial segmentation
Three-dimensional orbital wall modeling

ABSTRACT

Purpose: Three-dimensional orbital wall modeling is a time-consuming process because of the presence of pseudoforamina. We developed an automated three-dimensional modeling software to characterize the orbital wall, and evaluated it using data from fracture patients.
Methods: We first characterized the air and face regions using multiphase segmentation; the sinuses were segmented by applying morphological operations to air regions. Pseudoforamina of the orbital wall were offset with the segmented sinuses. Finally, the three-dimensional facial bone model, with orbital wall, was reconstructed from the segmented images.
Results: Ten computed tomography data sets were used to evaluate the proposed method. Results were compared with those obtained using the active contour model and manual segmentation. The process took 31.7 ± 8.0 s, which was 30–60 times faster than other methods. The average distances between surfaces obtained with the proposed method and those obtained with manual segmentation (normal side: 0.20 ± 0.06 mm; fractured side: 0.28 ± 0.10 mm) were approximately half those obtained using the active contour model.
Conclusions: Three-dimensional orbital wall models, which were very similar to the manually segmented models, were archived within 1 min using the developed software, regardless of fracture presence. The proposed method might improve the safety and accuracy of surgical procedures.

1. Introduction

Orbital fracture is a common facial trauma. Incidence of orbital fracture ranges from 18% to 50% of all cranio-maxillofacial traumas, reflecting differences in geographic region, injury mechanism, and study population (Chen and Chen, 2010). Injuries to the orbit can occur either independently or in combination with fractures of adjacent facial bones (Dubois et al., 2015). Failure to promptly recognize and treat these injuries can result in severe malfunction of human vision as well as cosmetic problems. Thus, the purpose of orbital reconstruction is to restore anatomically correct orbital volumes in order to avoid long-term complications. Since inadequate reconstruction can restrict normal function and facial aesthetics, reestablishment of exact orbital volume is key to reducing postinjury complications. However, the complex bony anatomy and limited intraoperative view make reconstruction challenging, even for skilled surgeons.

Over the years, advances in technology have aided orbital reconstructive surgical procedures. In particular, computer-assisted surgery — including preoperative planning, intraoperative

* Corresponding author. Center for Bionics, Korea Institute of Science and Technology, Division of Bio-Medical Science & Technology, KIST School, Korea University of Science and Technology, 5 Hwarang-ro 14-gil, Seongbuk-gu, Seoul, 02792, Republic of Korea.
** Corresponding author. Department of Plastic and Reconstructive Surgery, Biomedical Engineering Research Center, University of Ulsan College of Medicine, Seoul Asan Medical Center, 88 Olympic-ro 43-gil, Songpa-gu, Seoul, 05505, Republic of Korea.
E-mail addresses: hannah.kim7120@kist.re.kr (H. Kim), tgson@kist.re.kr (T.-g. Son), jeonghwan.lee85@gmail.com (J. Lee), hyun6596@nate.com (H.A. Kim), hccho@kist.re.kr (H. Cho), woosjeong.ps@gmail.com (W.S. Jeong), pschoi@amc.seoul.kr (J.W. Choi), junekim@kist.re.kr (Y. Kim).

https://doi.org/10.1016/j.jcms.2019.03.028
1010-5182/

navigation, and patient-specific implant design — is an effective tool in orbital reconstruction (Novelli et al., 2014; Shin et al., 2016), and is reported to improve outcomes for novice surgeons (Davis et al., 2016). A reliably constructed three-dimensional orbital model is essential for successful diagnosis and treatment of orbital diseases with computer-assisted surgery. However, bone segmentation of the orbit is challenging because of its anatomical traits — thin orbital walls and floors adjacent to paranasal sinuses. These regions are often misrepresented as holes called pseudoforamina (Holck et al., 1999) in three-dimensional models because of partial-volume effects or efforts to decrease radiation exposure.

Various approaches have been investigated in attempts to develop reliable segmentation and measurement methods, including threshold-based, image-based, atlas-based, and model-based segmentation. Typically, physicians perform orbital segmentation manually by carrying out thresholding with Hounsfield units, and tracing the orbital boundaries in computed tomography image slices. This method is accurate, and is considered the gold standard for evaluating other segmentation methods. However, it is time consuming and is sensitive to user error (interobserver and intraobserver errors). Image-based segmentation using mathematical models of intensity (Vese and Chan, 2002; Bresson et al., 2007; Kim et al., 2017) has been successfully used in many medical applications.

Unfortunately, most image-based segmentation methods used in orbital segmentation generate inadequate results containing leakages (similarly to threshold-based segmentation, which requires postprocessing to fix the results). Atlas-based segmentation uses manually labeled training images generated by a clinical expert as a template. By applying deformable registration and fusion to individual data sets, successful segmented images can be obtained (Metzger et al., 2013; Panda et al., 2014). This approach can be extended to orbital segmentation. However, results vary with respect to diversity in age and condition of the fracture, and the technique has clear limitations in that it cannot be used to properly visualize orbital bone defects (Metzger et al., 2013).

Model-based segmentation involves estimating the shape of the region of interest and placing it in the desired area. The shape is then deformed to fit the underlying data set, and the desired segmentation can be acquired (Cootes et al., 1995; Heimann and Meinzer, 2009). This method is more robust than atlas-based segmentation for measuring the volume of the orbital cavity (Wagner et al., 2016), but the orbital volume cannot accurately define anatomically important features in the orbital walls, such as the superior and inferior orbital fissures and the optic canal.

Some of the methods described have been employed using open-source or commercial software packages, such as ITK-SNAP (Kitware, New York, United States; Yushkevich et al., 2006), 3D slicer (Fedorov et al., 2012), YaDIV (Friese et al., 2011), and iPlan CMF (BrainLab, Munich, Germany). Unfortunately, these software programs may be inappropriate for use in orbital wall segmentation in order to generate a reliable three-dimensional orbital wall model. These programs are usually intended for general medical image processing, and the software features are not specialized for orbital segmentation, leading to failure or the need for intensive postprocessing. iPlan CMF employs an atlas-based method for facial bone segmentation, including segmentation of the orbital wall, but it cannot segment fractured orbital bone properly. Atlas-based segmentation is usually applied only to the normal orbit, and is manually corrected after mirroring the normal orbit with the fractured side (Gander et al., 2015; Schönegg et al., 2018).

The paranasal sinuses adjacent to the medial walls and floors of the orbits are empty space filled with air. When an orbital fracture occurs, the air spaces of the sinuses near the fracture are reduced, and this can be used to assess the patient's condition. Mustafa et al. (2010) tried virtual reconstruction of an orbital floor fracture using Mimics (Materialize Medical, Leuven, Belgium) by mirroring a three-dimensional maxillary sinus model of the normal side with the affected side and positioning it with a three-dimensional facial bone model. However, this cannot represent the actual condition of the fractured orbital wall, and the holes caused by pseudoforamina are not fully offset by the mirrored sinus.

This study aimed to investigate a practical, specialized segmentation approach for orbital wall modeling that could be applied to a fractured orbit. By combining an intensity-based multiphase segmentation method (Kim and Kang, 2012) with morphological image processing (Gonzalez and Woods, 2007), we aimed to achieve fast, accurate, and automatic three-dimensional orbital wall modeling on both the normal and affected sides. We incorporated the proposed method and its evaluation into an integrated software.

2. Materials and methods

2.1. Three-dimensional orbital wall modeling: proposed method

Normally, the intensity of facial bone CT ranges from +700 to +3000 Hounsfield units. The orbital wall is the thinnest bone of the human body, and it is difficult to generate a three-dimensional model of the orbital wall using simple threshold-based segmentation because there would be pseudoforamina from both the normal and fractured orbits, as indicated in Fig. 1. Moreover, even if a surgeon knows which side is fractured, it is hard to find the defect region in the three-dimensional model. To solve this problem, we proposed an automatic three-dimensional orbital wall modeling method using paranasal sinus segmentation. The paranasal sinuses adjacent to the medial wall and floor of the orbits are empty space filled with air. When an orbital fracture occurs, the air spaces of the sinuses near the fracture are reduced because the orbital wall is depressed, or the air spaces are filled with blood. Therefore, we segmented the air spaces in the paranasal sinuses first, and these were used to fill misrepresented holes caused by pseudoforamina in the orbital wall.

Fig. 2 shows the overall procedure for the proposed method, which comprises the following steps: (1) initial multiple region segmentation, (2) facial region extraction, (3) paranasal sinus segmentation, and (4) orbital wall segmentation. After these segmentation procedures were performed on each axial computed tomography image, the three-dimensional facial bone model with orbital wall was reconstructed to generate a three-dimensional surface model from the segmented images. Fig. 3 shows a snapshot from our developed software.

Initially, we obtained labeled images of different regions from the computed tomography image using adaptive global maximum clustering (Kim and Kang, 2012). This is a multiphase segmentation algorithm for separating the histogram of the input image into several clustered regions. Adaptive global maximum clustering can be used to determine the number of distinct regions and segment the multiple regions automatically. After applying adaptive global maximum clustering to the entire area of the input computed tomography image, labeled images were obtained in which each clustered region's pixels had similar intensities. The air, soft tissue, and bone regions were relatively distinct from each other, so the output comprised three labels.

In the next step, the facial region was extracted before paranasal sinus segmentation. Since the sinuses are empty spaces filled with air, those regions contained the air label from the first step. However, air exists inside and outside of the patient, so the facial region was extracted to separate the paranasal sinuses and exernal air regions. To extract the facial region, the non-air labels were merged,

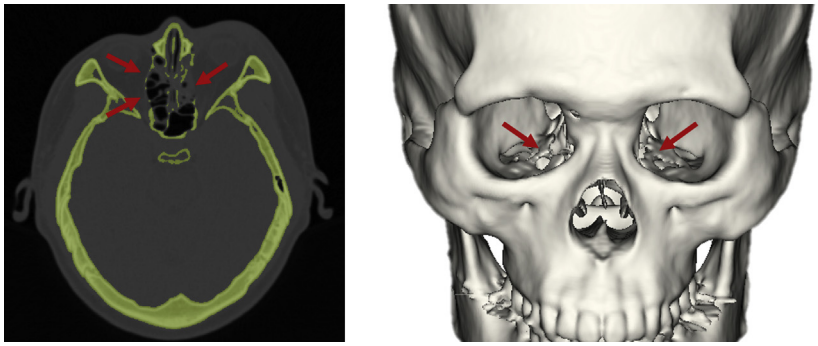

Fig. 1. Unsuccessful segmentation result using the threshold-based method: this patient has a fractured medial wall of the left orbit, but there are many holes in both orbits because of pseudoforamina, as indicated by the red arrows.

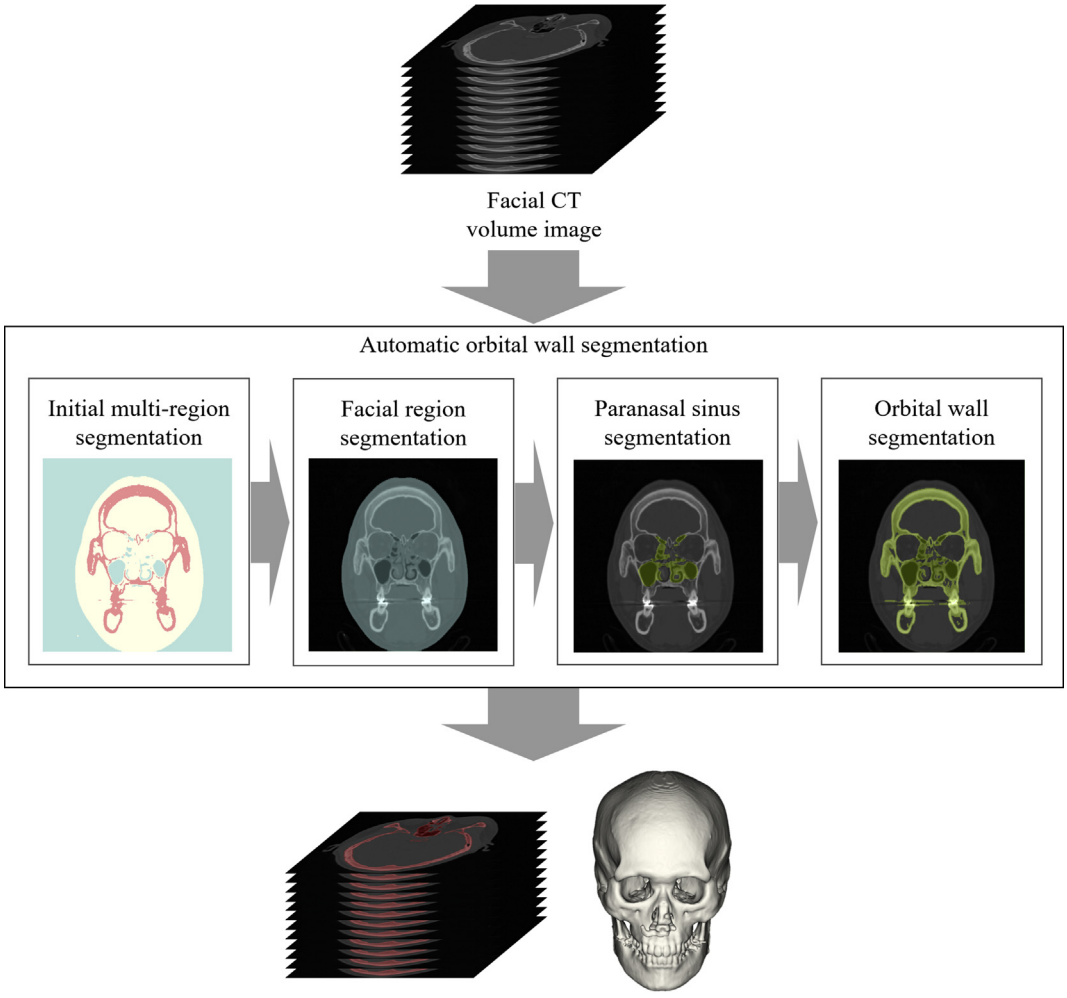

Fig. 2. Overall flow of the proposed three-dimensional orbital wall modeling method. 3D, three-dimensional; CT, computed tomography.

and the facial region was extracted by filling the holes of the merged image.

The air regions inside the facial region were then extracted for sinus segmentation. The sinus regions included both the air label of the first step and the facial region, so could be easily determined. However, because the paranasal sinus is divided into several spaces, morphological dilation was performed to integrate nearby spaces into one. Because there were some errors in classifying regions from the air labeling, the dilated paranasal sinus region was extracted by searching the first region, in the head-to-chin direction, using a volume-of-interest defined central 40% of each axis. The final nondilated paranasal sinus regions were obtained by overlapping the dilated sinus regions and the air regions inside the facial region.

Fig. 3. Screen capture of the proposed automatic software for three-dimensional orbital wall modeling.

Finally, the segmented paranasal sinus regions were gathered into one region using a morphological closing operation, and the gathered sinus region and the initial bone region were combined to supplement the medial and floor parts of the orbit. The initial bone region was defined by thresholding the original computed tomography image using the +700 to +3000 Hounsfield units range for human bone. The three-dimensional model of the orbital wall was reconstructed by matching cubes from the segmented axial images (Lorensen and Cline, 1987).

2.2. Data acquisition

Ten computed tomography data sets of the head were used to evaluate the proposed modeling method. The data sets were acquired from ten patients, 26–64 years old, in the plastic and reconstructive surgery department of a major medical center in the Republic of Korea, from 2014 to 2017. The data sets consisted of nine with orbital fracture on one side and one without the fracture as a control. The fractures varied and included orbital floor fracture, medial wall fracture, and complex fracture of the floor and medial wall. The computed tomography data sets comprised slice images ranging from 171 slices to 246 slices; each slice image was 512 × 512 pixels. The pixel spacing for each data set varied between 0.30 × 0.30 mm and 0.46 × 0.46 mm, and the slice thickness was 1 mm.

2.3. Comparison materials

1. Manual segmentation

The models chosen for the evaluation were manually segmented and reconstructed three-dimensionally by two biomedical engineers, using commercial software (Mimics Materialize; Materialize Medical, Leuven, Belgium). An expert clinician at the Seoul Asan Medical Center (Seoul, Republic of Korea) confirmed the results. The engineers initially segmented the facial bones with Hounsfield unit thresholding and then manually supplemented the orbital wall regions slice by slice.

2. Conventional automatic segmentation: active contour model

Conventional automatic segmentation, using an algorithmic level set-based active contour model (Kim et al., 2017), was implemented under the same conditions for purposes of comparison with the proposed method. The active contour model, widely used in medical imaging, is used to segment various regions from soft tissue to bone (Zhou et al., 2016; Ilunga-Mbuyamba et al., 2017; Patel et al., 2017). It has performed well in segmenting zygomatic bone (Gibelli et al., 2018) and paranasal sinuses (Bui et al., 2015; Deng et al., 2017), which are very close to the orbital wall. Among the many variations of active contour model, we chose the two-stage level set-based active contour model (Kim et al., 2017) for segmenting the orbital wall. In the first stage, trial segmentation based on intensity and internal shape fitting was performed. In the second stage, fine segmentation was achieved by comparing and correcting the trial segmentation with the fitted shape. For each data set, the same volume of interest and initial bone region used in the proposed method were assigned to the comparative method. The segmentation results were reconstructed three-dimensionally in the same way as in the proposed method.

2.4. Evaluation

To evaluate the speed and accuracy of the proposed method, we measured the time spent segmenting the orbital wall for manual segmentation, the active contour model, and the proposed method. We also calculated the surface distances from the three-dimensional orbital wall model obtained by the proposed method and the active contour model to the manually created model. Because our target was not the entire facial bone, we extracted the three-dimensional orbital wall models from the results for each

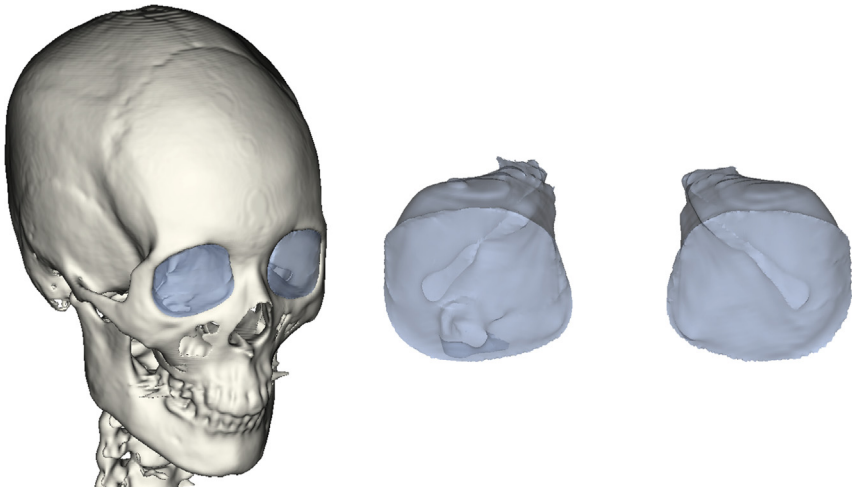

Fig. 4. Three-dimensional orbital cavity model developed with mesh filling of holes in the three-dimensional orbital wall model (data set 1).

method before measuring the distance, in order to more accurately evaluate the target.

The three-dimensional orbital wall model was acquired after creating a sphere by clicking two points in the orbit and spreading rays from the sphere to the orbital wall in the three-dimensional facial bone model. Identical spheres were created for each data set and were applied equally to the results of all segmentation methods, to prevent inconsistent results caused by user input. Moreover, the volume of each three-dimensional orbital wall model was measured by generating a three-dimensional orbital cavity model (Fig. 4). The three-dimensional orbital cavity model was obtained by applying a mesh hole filling operation to the three-dimensional orbital wall model using the open-source library MeshFix, 2018 (https://sourceforge.net/projects/meshfix; accessed December 18, 2018).

3. Results

Fig. 5 presents plots of the average processing time for orbital wall segmentation using each method. The proposed method produced the lowest average processing time (31.7 s) when compared with the active contour model and manual methods. The average times spent for manual segmentation and segmentation with the active contour model were 27 min 57 s and 34 min 49 s, respectively.

The average and maximum distances from the surfaces of the three-dimensional orbital wall models acquired by the active contour model and the proposed method to the surfaces obtained with the chosen manual segmentation model for every test data set are presented in Table 1. Fig. 6 shows a comparison of the average surface distances and maximal surface distances for all data sets. When using the active contour model, the average distances to the corresponding manual segmentation model surface were 0.75 ± 0.15 mm and 0.80 ± 0.10 mm for the normal and fractured sides, respectively. The average maximum distances were 5.12 ± 0.15 mm for the normal side and 5.32 ± 0.93 mm for the fractured side. The proposed method resulted in average distances of 0.20 ± 0.06 mm and 0.28 ± 0.10 mm for the normal and fractured sides, respectively. Moreover, the proposed method yielded average

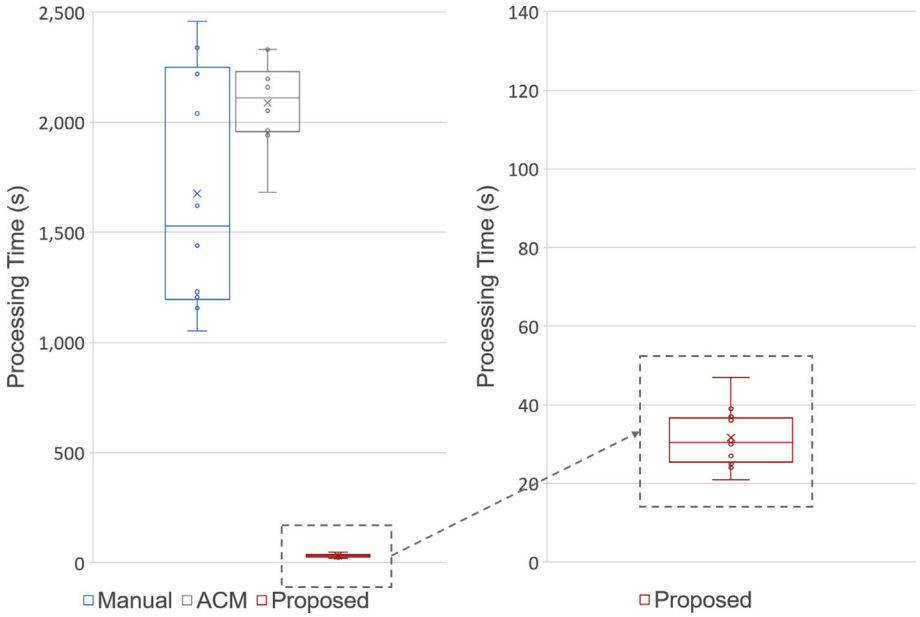

Fig. 5. Average processing times for segmenting the orbital wall, by method: (left) processing times for all methods; (right) detailed view of proposed method. ACM, active contour model.

Table 1
Surface distances for three-dimensional orbital wall models (mm) — the active contour model (ACM) and the proposed method.

Data set	Defect	Side	ACM (Kim et al., 2017)		Proposed method	
			Average distance (mm)	Maximum distance (mm)	Average distance (mm)	Maximum distance (mm)
1	Right floor	Normal	0.53	3.88	0.35	1.68
		Fractured	0.67	5.24	0.47	4.72
2	Right floor and medial wall	Normal	0.67	4.03	0.25	2.65
		Fractured	0.71	7.04	0.31	4.50
3	Right floor and medial wall	Normal	0.61	4.29	0.23	2.05
		Fractured	0.88	5.22	0.39	3.77
4	Left medial wall	Normal	0.65	3.34	0.13	2.62
		Fractured	0.73	3.91	0.22	3.88
5	Left floor and medial wall	Normal	0.76	4.63	0.14	3.05
		Fractured	0.83	4.93	0.20	3.28
6	Left medial wall	Normal	1.07	7.02	0.17	3.37
		Fractured	0.95	5.99	0.14	3.26
7	Left floor and medial wall	Normal	0.79	6.00	0.21	1.69
		Fractured	0.87	5.11	0.24	2.41
8	Left medial wall	Normal	0.61	4.44	0.17	2.96
		Fractured	0.66	4.91	0.19	3.32
9	Left floor and medial wall	Normal	0.85	5.99	0.16	3.41
		Fractured	0.87	5.56	0.32	4.85
10	Normal	Normal	0.82	6.45	0.19	2.90
		Normal	0.92	6.27	0.23	4.85

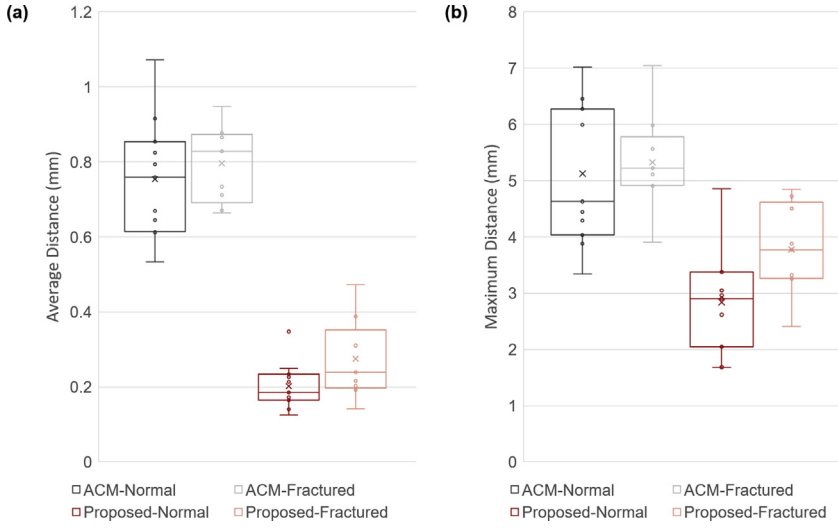

Fig. 6. Comparisons of the distances between the surfaces obtained with three-dimensional modeling methods (active contour model [Kim et al., 2017] and the proposed method) and surfaces obtained with manual segmentation: (a) average distance; (b) maximum distance. ACM, active contour model.

maximum distances of 2.84 ± 0.86 mm and 3.77 ± 0.76 mm for the normal and fractured sides, respectively (see Table 2).

Fig. 7 illustrates the differences between the orbital volumes obtained with the proposed method and the active contour model and those obtained with manual segmentation. For the active contour model, the volume differences were 1.48 ± 1.41 cm^3 and 2.13 ± 2.19 cm^3 for the normal and fractured sides, respectively. The proposed method resulted in average volume differences of 0.70 ± 0.47 cm^3 and 1.31 ± 1.50 cm^3 for the normal and fractured sides, respectively.

Table 2
Surface distances for three-dimensional orbital wall models (%) — the active contour model (ACM) and the proposed method.

	ACM (Kim et al., 2017)		Proposed	
	Normal (%)	Fractured (%)	Normal (%)	Fractured (%)
0–1 mm	82.1	79.3	98.4	94.8
1–2 mm	12.0	13.9	1.2	3.7
2–3 mm	3.6	4.2	0.3	1.1
Over 3 mm	2.3	2.5	0.1	0.4

Each row represents the average percentage of vertices in the specified range of surface distances over all vertices in the three-dimensional orbital models obtained with the active contour model (ACM) and the proposed method.

4. Discussion

The proposed method shortened the orbital wall modeling time by 30–60 times (over 98% reduced), compared with the manual method and the comparative automatic method (active contour modeling). In the case of an orbital fracture, it is difficult to perform manual segmentation because the fractured orbital wall is not closed, and the boundary is ambiguous. For example, the average times required for manual segmentation were 24.0 min for the normal data (data set 10) and 28.2 min on average for the nine orbital fracture data sets; the fracture data set time was 15% longer than that observed for normal data. However, when the proposed

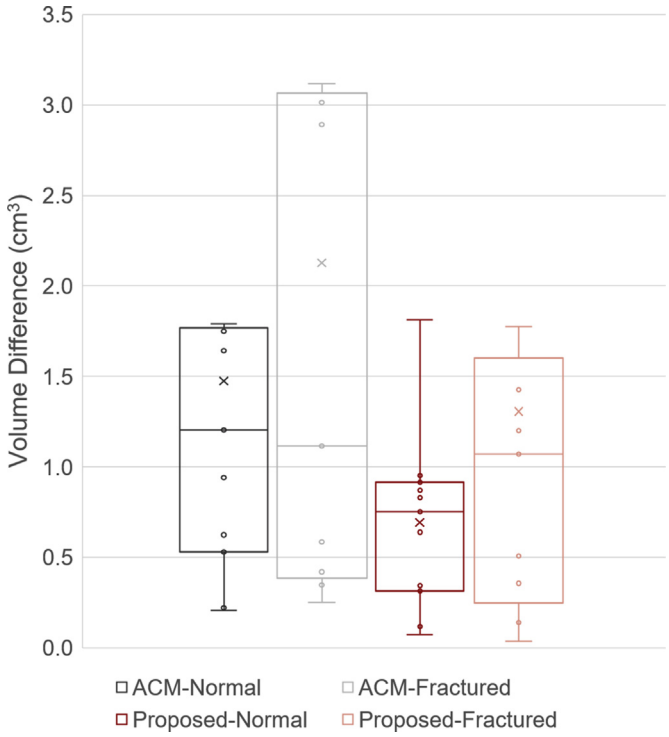

Fig. 7. Comparisons of the differences in orbital volumes obtained with three-dimensional modeling methods (active contour model [Kim et al., 2017] and the proposed method) and those obtained with manual segmentation. ACM, active contour model.

method was used, the time required for normal data was 31.0 s, and the average time for the fracture data sets was 31.8 s — an increase of 2.4%. Therefore, the presence of orbital fracture did not substantially affect the time required for the proposed method.

All the evaluated segmentation methods aimed at modeling the orbital wall, including manual segmentation, showed inconsistent results when compared with volume images, as shown in Fig. 8. The active contour model tended to detect strong edges, such as contours, near the sinuses (Fig. 8c). However, the active contour model missed some bone regions or oversegmented soft tissue regions, which have intensities similar to those of the adjacent areas (white arrows). In contrast, these over- and undersegmentation issues were not observed with the proposed method (Fig. 8d). It was therefore difficult to measure the accuracy of the segmentation methods by calculating agreement with the manual method at the volume image level. It was also difficult to determine the measurement area in the image, because the orbital wall is contiguous with other facial bones. For these reasons, we evaluated the performance of the segmentation methods by measuring the distances between the surfaces of the three-dimensional orbital wall models and those of the manual segmentation models.

The surface distance for the proposed method was, on average, less than 0.3 mm for fractured orbital bone, and both means and standard deviations were lower than those observed with the active contour model for both normal and fractured sides. In addition, more than 15% of the vertices acquired with the proposed method were located within 1 mm of those acquired using manual segmentation for both the normal and fractured orbitals. In the three-dimensional orbital model generated by the proposed method, 99.6% of vertices on the normal side and 98.5% of the vertices on the affected side were located within 2 mm, and showed little difference from the chosen manual segmentation model (see Table 2).

Fig. 9 shows differences in the surface shape results between the active contour model and the proposed method. The proposed method produced a more regular and cleaner model than did the active contour model, and the overall difference from the manual segmentation method was lower for the proposed method than for the active contour model. The overall shapes resulting from the proposed method were almost identical to the manually created models, and that they exhibited low surface distances. Because the surface difference directly affects the measurement of the orbital volume, the proposed method exhibited smaller differences from the manual segmentation results on both the normal and fractured sides than did the active contour model.

Both the active contour model and the proposed method had larger surface distances and volume differences on the fractured side than on the normal side. To investigate the cause of this, we measured the surface distance of the fracture area for data set 1. The surface distances in the fracture area were 1.93 mm for the active contour model and 1.03 mm for the proposed method. These distances were about twice as large as those for the entire orbital wall for data set 1, which were 0.67 mm and 0.47 mm, respectively. Therefore, the surface distances for the fractured side appeared to have increased because of errors occurring in the fracture area.

The fracture area needs to be considered when biomedical engineers evaluate manual segmentation data. Because the orbital bone was very thin, fractured segments of the orbital wall were not clearly visible, and the boundary of the fracture area could not be clearly identified; the surgeon had to confirm the results. Despite

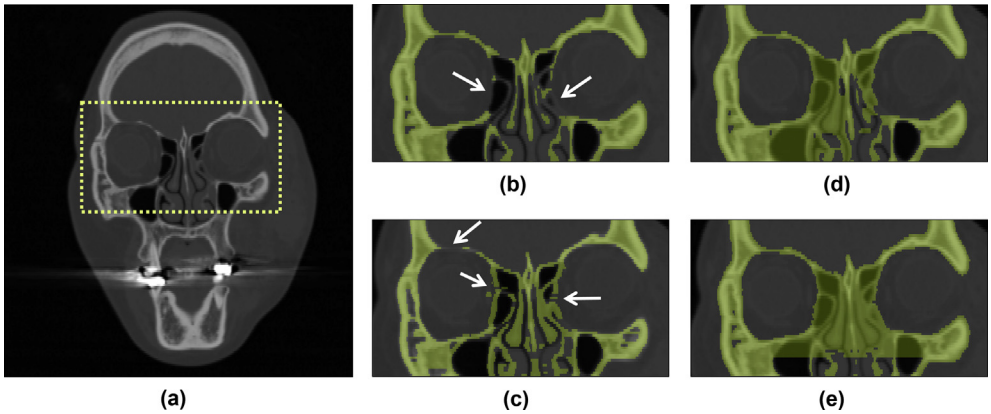

Fig. 8. Comparisons of various segmentations in two-dimensional slice images: (a) original image; (b) Hounsfield unit thresholding method segmentation; (c) active contour model segmentation (Kim et al., 2017); (d) proposed segmentation method; (e) manual segmentation. White arrows indicate over- and undersegmented regions.

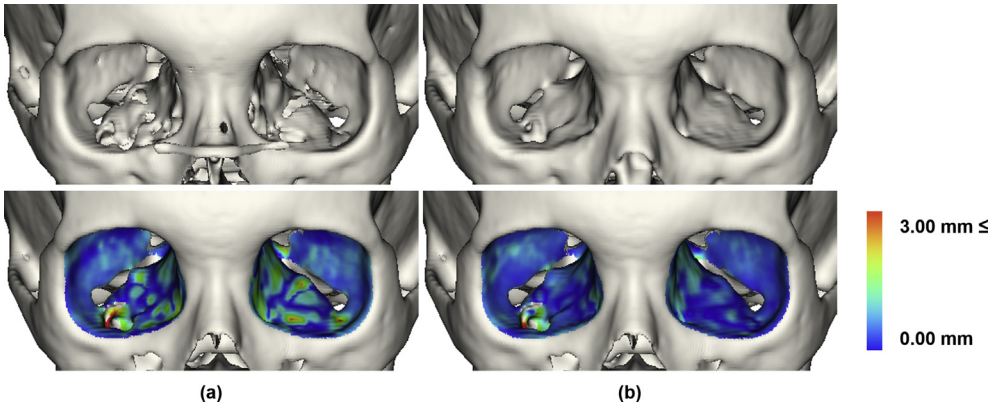

Fig. 9. First row: three-dimensional models of orbital wall obtained by automated methods (active contour model [Kim et al., 2017] and the proposed method); second row: color map based on the distances to the surfaces of the manually created model (data set 1). The right orbital floor was fractured. (a) active contour model (ACM) (Kim et al., 2017); (b) proposed method.

these issues, the proposed method resulted in smaller average surface distances and volume differences than did the active contour model.

The proposed method aimed to model the orbital wall rather than the inner region of the orbit, which is the focus of several other studies (Wagner et al., 2016; Jansen et al., 2016; Dahl et al., 2016; Hsung et al., 2018; Nilsson et al., 2018). In addition, use of the proposed method enabled archiving of the three-dimensional orbital wall model in less than a minute, even for patients with fractures. We expect that the proposed three-dimensional orbital wall model can be used for orbital volume measurement, as well as in surgical procedures for diagnosis and measurement of the fracture area (Fig. 10a), design of patient-specific implants (Fig. 10b), and in surgical navigation, to improve safety and accuracy.

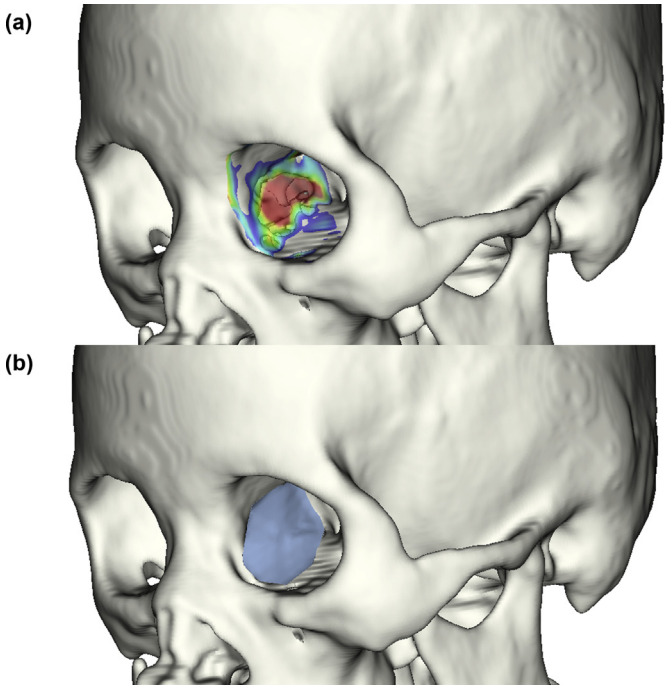

Fig. 10. Application of the three-dimensional orbital wall model acquired by the proposed method: (a) orbital fracture detection obtained by mirroring and registration of the normal orbit to the orbit of the affected side; (b) patient-specific plate based on the detected area (data set 9).

5. Conclusion

In this study we presented an automatic, three-dimensional orbital wall modeling method using paranasal sinus segmentation. The method was able to archive three-dimensional orbital wall models accurately within 1 min, regardless of whether orbital fracture was present. The efficiency in terms of processing time and the accuracy of the proposed method were verified by comparison with the most advanced conventional method (active contour model) and with manual segmentation, which is the standard approach. The proposed method has difficulties in distinguishing between old and acute blowout fractures, but these can be solved by examination of the correlation with clinical symptoms and medical history. Based on our results, three-dimensional orbital wall models obtained with the proposed method can be widely applied to all stages of orbital reconstruction surgery.

Acknowledgements

This work was supported by the KIST Institutional program, Korea Institute of Science and Technology, Republic of Korea (2V05810, 2E27990), and the research was supported by a grant from the Korea Health Technology R&D Project, Korea Health Industry Development Institute (KHIDI), Ministry of Health & Welfare, Republic of Korea (grant number: HI18C1224).

References

Bresson X, Esedoğlu S, Vandergheynst P, Thiran JP, Osher S: Fast global minimization of the active contour/snake model. J Math Imaging Vis 28: 151–167, 2007
Bui NL, Ong SH, Foong KWC: Automatic segmentation of the nasal cavity and paranasal sinuses from cone-beam CT images. Int J Comput Assist Radiol Surg 10: 1269–1277, 2015
Chen CT, Chen YR: Update on orbital reconstruction. Curr Opin Otolaryngol Head Neck Surg 18: 311–316, 2010
Cootes TF, Taylor CJ, Cooper DH, Graham J: Active shape models — their training and application. Comput Vis Image Underst 61(38–59), 1995
Dahl VA, Einarsson G, Darvann TA, Hermann NV, Hove HB, Kakimoto N, et al: Automatic measurement of orbital volume in unilateral coronal synostosis. In: 2016 IEEE 13th International symposium on biomedical imaging. ISBI, 889–893, 2016
Davis KS, Vosler PS, Yu J, Wang EW: Intraoperative image guidance improves outcomes in complex orbital reconstruction by novice surgeons. J Oral Maxillofac Surg 74: 1410–1415, 2016
Deng Z, Kitamura T, Matsushiro N, Nishimura H, Zhu Z, Xu M, et al: Semi-automatic segmentation of paranasal sinuses from CT images using active contour with group similarity constraints. In: The International conference on Innovation in medicine and healthcare 2017; 2017, 89–98, 2017
Dubois L, Steenen SA, Gooris PJJ, Mourits MP, Becking AG: Controversies in orbital reconstruction — I. Defect-driven orbital reconstruction: a systematic review. Int J Oral Maxillofac Surg 44: 308–315, 2015

Fedorov A, Beichel R, Kalpathy-Cramer J, Finet J, Fillion-Robin JC, Pujol S, et al: 3D slicer as an image computing platform for the Quantitative Imaging Network. Magn Reson Imaging 30: 1323–1341, 2012
Friese KI, Blanke P, Wolter FE: YaDiV — an open platform for 3D visualization and 3D segmentation of medical data. Vis Comput 27: 129–139, 2011
Gander T, Essig H, Metzler P, Lindhorsts D, Dubois L, Rücker M, et al: Patient specific implants (PSI) in reconstruction of orbital floor and wall fractures. J Craniomaxillofac Surg 43: 126–130, 2015
Gibelli D, Cellina M, Gibelli S, Oliva AG, Termine G, Pucciarelli V, et al: Assessing symmetry of zygomatic bone through three-dimensional segmentation on computed tomography scan and 'mirroring' procedure: a contribution for reconstructive maxillofacial surgery. J Craniomaxillofac Surg 46: 600–604, 2018
Gonzalez RC, Woods RE: Morphological operations. Digital image processing, 3rd ed. Upper Saddle River, New Jersey, United States: Prentice Hall, 630–639, 2007
Heimann T, Meinzer HP: Statistical shape models for 3D medical image segmentation: a review. Med Image Anal 13: 543–563, 2009
Holck DE, Boyd Jr EM, Ng J, Mauffray RO: Benefits of stereolithography in orbital reconstruction. Ophthalmology 106: 1214–1218, 1999
Hsung TC, Lo J, Chong MM, Goto TK, Cheung LK: Orbit segmentation by surface reconstruction with automatic sliced vertex screening. IEEE Trans Biomed Eng 65: 828–838, 2018
Ilunga-Mbuyamba E, Avina-Cervantes JG, Cepeda-Negrete J, Ibarra-Manzano MA, Chalopin C: Localized active contour model with background intensity compensation applied on automatic MR brain tumor segmentation. Neurocomputing 220: 84–97, 2017
Jansen J, Schreurs R, Dubois L, Maal TJ, Gooris PJ, Becking AG: Orbital volume analysis: validation of a semi-automatic software segmentation method. Int J Comput Assist Radiol Surg 11: 11–18, 2016
Kim S, Kang M: Multiple-region segmentation without supervision by adaptive global maximum clustering. IEEE Trans Image Process 21: 1600–1612, 2012
Kim S, Lee D, Park S, Oh KS, Chung SW, Kim Y: Automatic segmentation of supraspinatus from MRI by internal shape fitting and autocorrection. Comput Meth Progr Biomed 140: 165–174, 2017
Lorensen WE, Cline HE: Marching cubes: a high resolution 3D surface construction algorithm. ACM Siggraph Comput Graph 21: 163–169, 1987
MeshFix. Available at: https://sourceforge.net/projects/meshfix
Metzger MC, Bittermann G, Dannenberg L, Schmelzeisen R, Gellrich NC, Hohlweg-Majert B, et al: Design and development of a virtual anatomic atlas of the human skull for automatic segmentation in computer-assisted surgery, preoperative planning, and navigation. Int J Comput Assist Radiol Surg 8: 691–702, 2013
Mustafa SF, Key SJ, Evans P, Sugar AW: Virtual reconstruction of defects of the orbital floor using the morphometry of the opposite maxillary sinus. Br J Oral Maxillofac Surg 48: 392–393, 2010
Nilsson J, Nysjö J, Carlsson AP, Thor A: Comparison analysis of orbital shape and volume in unilateral fractured orbits. J Craniomaxillofac Surg 46: 381–387, 2018
Novelli G, Tonellini G, Mazzoleni F, Bozzetti A, Sozzi D: Virtual surgery simulation in orbital wall reconstruction: integration of surgical navigation and stereolithographic models. J Craniomaxillofac Surg 42: 2025–2034, 2014
Panda S, Asman AJ, Khare SP, Thompson L, Mawn LA, Smith SA, et al: Evaluation of multiatlas label fusion for in vivo magnetic resonance imaging orbital segmentation. J Med Imaging (Bellingham) 1: 024002, 2014
Patel A, van Ginneken B, Meijer FJ, van Dijk EJ, Prokop M, Manniesing R: Robust cranial cavity segmentation in CT and CT perfusion images of trauma and suspected stroke patients. Med Image Anal 36: 216–228, 2017
Schönegg D, Wagner M, Schumann P, Essig H, Seifert B, Rücker M, et al: Correlation between increased orbital volume and enophthalmos and diplopia in patients with fractures of the orbital floor or the medial orbital wall. J Craniomaxillofac Surg 46: 1544–1549, 2018
Shin HS, Kim SY, Cha HG, Han BL, Nam SM: Real time navigation-assisted orbital wall reconstruction in blowout fractures. J Craniofac Surg 27: 370–373, 2016
Vese LA, Chan TF: A multiphase level set framework for image segmentation using the Mumford and Shah model. Int J Comput Vis 50: 271–293, 2002
Wagner ME, Gellrich NC, Friese KI, Becker M, Wolter FE, Lichtenstein JT, et al: Model-based segmentation in orbital volume measurement with cone beam computed tomography and evaluation against current concepts. Int J Comput Assist Radiol Surg 11: 1–9, 2016
Yushkevich PA, Piven J, Hazlett HC, Smith RG, Ho S, Gee JC, et al: User-guided 3D active contour segmentation of anatomical structures: significantly improved efficiency and reliability. Neuroimage 31: 1116–1128, 2006
Zhou S, Wang J, Zhang S, Liang Y, Gong Y: Active contour model based on local and global intensity information for medical image segmentation. Neurocomputing 186: 107–118, 2016